A priori Design of a Photoreactor for the Chlorination of Ethane

A three-dimensional radiation model coupled with two-dimensional mass balances for the intervening chemical species is solved for the photochemical chlorination of ethane. The analysis was carried out using the full mechanistic kinetic sequence and employing polychromatic radiation for a process conducted in a tubular reactor placed inside an elliptical reflector.

Theoretical predictions were compared with bench-scale experiments and showed excellent agreement. Using the validated model, computational experiments were conducted to explore the influence of reactor design and operational parameters upon the degree of chlorination. Dichlorination reactions were also added to the kinetic model to analyze reactor behavior from the viewpoint of selectivity. The *a priori* design method described can be applied from first principles and requires no experimentally adjustable parameters.

M. A. Clariá, H. A. Irazoqui, A. E. Cassano
Instituto de Desarrollo Tecnológico para la Industria Química; Universidad Nacional del Litoral and Consejo Nacional de Investigaciones Científicas y Técnicas
Santa Fe, 3000 Argentina

Introduction

A method proposed for the design of a photoreactor may ascertain its quality by producing good results even in the presence of the three following operating situations:

1. Prediction of reactor behavior for multiple-step or chain reactions
2. Modeling of a reactor with a rather complex radiation field
3. Inclusion of heterogeneities in the reacting system, for instance, in a gas-liquid reaction

In this work we develop an *a priori* design of a reactor for a homogeneous photochemical chain reaction, in a system with an elliptical reflector, thus addressing the first two problems. The third difficulty was dealt with in a separate work (Alfano, 1984).

To achieve the scope indicated in situation 1 we studied the gas-phase photochemical monochlorination of ethane in a tubular cylindrical reactor. To provide the conditions for a decisive answer with respect to situation 2 we chose a difficult setup to model: a cylindrical reflector of elliptical cross section with a tubular lamp located at one of its focal axes and the reactor tube at the other axis. This is perhaps the most practical tubular reactor system for laboratory and bench-scale work in continuous, single-phase experiments, although in many cases its applicability to large-scale purposes may be questioned. Success in modeling its radiation field should provide the necessary confidence to extend the methodology to simpler situations.

The system, known as an elliptical photoreactor, is shown schematically in Figure 1. For a chain reaction it has never before been strictly modeled from first principles without the use of experimentally adjustable parameters. On the other hand, it has been extensively used in experimental work since the early studies of Baginsky (1951). We may cite, for example, Huff and Walker (1962), Cassano and Smith (1966, 1967), Jacob and Dranoff (1969), Matsuura et al. (1969), Boval and Smith (1970), Matsuura and Smith (1970), Harada et al. (1971), Zolner and Williams (1972), Williams and Yen (1973), and Williams (1976), to mention only a few applications.

A good radiation model is always necessary because the rate of reaction of the first step (initiation), in any single-photon-activated photochemical reaction is proportional to the local volumetric rate of energy absorption (LVREA), as was shown by Irazoqui et al. (1976). The LVREA is proportional to the radiation energy flux density, which is a local property of the radiation field inside the photoreactor. In any practical reactor this field is necessarily strongly nonuniform. This nonuniformity is due to the attenuation produced by the radiation absorption by reactants (and sometimes inerts and products) and the geomet-

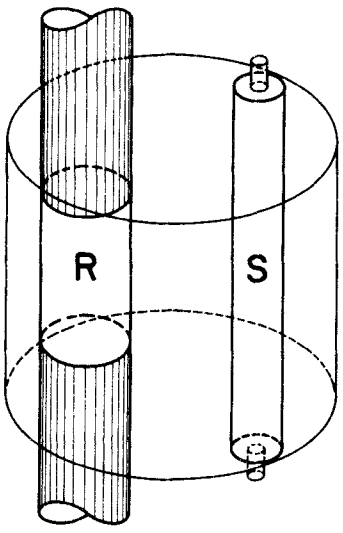

Figure 1. Elliptical photoreactor.
R, reactor; S, radiation source.

rical characteristics of the reactor–radiation-emitting system. In segregated flow reactors the effect of these nonuniformities is even more severe; thus, the existence of a nonuniform velocity profile incorporates additional complexity in the problem.

Several attempts have been made to model such a system. We can mention the work performed by Dolan et al. (1965) where a radial incidence model was used; by Matsuura and Smith (1970) with a bidimensional, incidence, diffuse radiation model; and by Zolner and Williams (1971), introducing a three-dimensional, incidence, diffuse radiation model. All of these models needed one or two experimentally adjustable parameters, which is an intrinsic characteristic of all incidence models. Cerdá et al. (1973) applied an emission model to a diactinic (nonabsorbing) elliptical photoreactor as an extension of the extense source model first proposed by Irazoqui et al. (1973) for a diactinic annular photoreactor. This was the first proposal of a three-dimensional emission model with no experimentally adjustable parameters.

Although some indications exist as to the ability of the extense source model to reproduce the behavior of a reactor (Cerdá et al., 1977), no test with complex reactions has yet been performed. On the contrary, in spite of the fact that this model is recognized as the most rigorous available (Gebhard, 1978; Spadoni et al., 1980), it has always been said that its complexity may preclude its use in practical situations.

In this work we solved the problem with the reactor and the reaction modeled with almost no simplifications, using the best-known mechanism and the specific microkinetic constants taken from results well established in the literature. No overwhelming computational problems were encountered. However, in order to work without the necessity of using a three-dimensional mass balance for the reactor (due to the presence of angular asymmetries in the radiation field), some design restrictions had to be observed, as shown by De Bernardez and Cassano (1982). All these provisions were taken into account in this work.

Through the analysis of initial computer simulation results, the solution of the complete problem also showed that there exists reliable evidence for some significant simplifications of the design methodology.

Afterward, we compared predictions of the model with experimental data obtained under precisely controlled experiments with the object of: (1) verifying the quality of the proposed model under severe testing conditions, and (2) showing the possibility of performing a satisfactory photoreactor design using true microkinetic (mechanistic) rate constants and a radiation modeling that requires only reliable information provided by carefully evaluated manufacturing specifications regarding the lamp, the reflector, and the reactor. To do so, bench-scale results were obtained working with polychromatic radiation (also included in the analysis) and the reaction between ethane and chlorine. Nitrogen was used as a diluent to avoid excessive heating of the reactor.

Once the applicability of the design method was confirmed, a detailed study of the reaction and the reactor behavior was made by additional computer simulation runs, providing much more insight about the performance and parametric sensitivity of the system.

The important practical application of this work lies in the fact that if in a reactor such as the one dealt with, our method verifies that the kinetic mechanisms and rate constants that have been published are not laboratory-dependent (i.e., they are appropriate to accurately predict conversions *a priori*), then using this approach it will be possible to make any change of scale for any desired size or geometry. For the new situation, which could easily be on the industrial scale, it will be necessary to model only the new radiation field. With this purpose one could follow an entirely similar procedure to the one described in this paper for the elliptical case.

Modeling of Local Volumetric Rate of Energy Absorption

Irazoqui et al. (1976) showed that the initiation rate of a photochemical reaction activated by a single photon absorption may be written as follows:

$$R_{init} = \int \Phi_\nu e^a_\nu \, d\nu \tag{1}$$

Here, Φ_ν is the primary quantum yield and e^a_ν is the local volumetric rate of energy absorption (LVREA). The value of e^a_ν is a function of the distribution of the radiation field and the chlorine concentration in space as well as of other physical and geometrical parameters of the source-reactor system. To predict the radiation field we made use of the extense source model with voluminal emission (Irazoqui et al., 1973, 1976; Cerdá et al., 1973, 1977). From now on it will be called the VEES (voluminal emission extense source) model, indicating that it physically represents a lamp whose emission is produced by the volume of the tube, as opposed to other sources with superficial emission, such as fluorescent lamps. No use of the linear models was made because it has been shown that the existing formulation is useful only to predict the field produced by direct radiation (Alfano et al., 1984). The rate of initiation is represented by:

$$R_{init} = \int_{\nu=0}^{\nu=\infty} \Phi_\nu \alpha_\nu C_{Cl_2} |\underset{\sim}{q}_\nu| \, d\nu \tag{2}$$

where α_ν is the chlorine absorption coefficient.

Since we have a reflecting surface, the modulus of the radiation energy flux density $|\underset{\sim}{q}_\nu|$ should be obtained by adding the

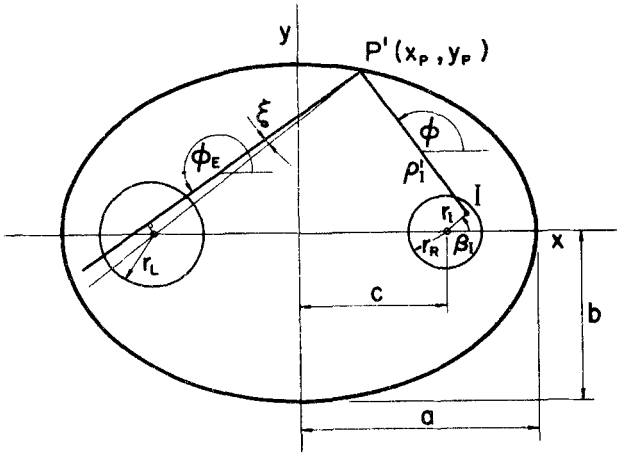

Figure 2. Variables involved in theoretical analysis of indirect radiation.

contributions of both direct incident radiation and indirect or reflected incident radiation with one or more reflections at the mirror wall. At this point we will introduce the first simplification of the problem. Cerdá et al., (1977) showed that for many elliptical photoreactors the indirect radiation with only one reflection accounts for 80 to 95% of the total radiation. Later, De Bernardez and Cassano (1982) made a study of the azimuthal asymmetries in these systems, mainly originated in the existence of direct incident radiation and the presence of a radiation-absorbing reactor of significant size in the trajectories of the indirect contributions. They developed design criteria under which angular asymmetries can be neglected. Under these conditions the mass balances will also be simplified because they can be written in only two dimensions. The key parameter is the ratio of r_R to r_L, the cylindrical radial coordinates of reactor and source, respectively. The established conditions can easily be achieved in bench-scale apparatus and they were taken into account for this study of the reactor ($e \leq 0.4$, $c/r_L > 20$, and $rR/r_L \leq 0.5$).

Under these terms the value of the modulus of the radiation energy density flux vector at any point I inside the reactor, Figure 2, considering the attenuation produced by the absorbing reactant can be written as follows:

$$|dq_\nu| = \Gamma_{Rf,\nu} T_{R,\nu} \frac{E_\nu}{4\pi V_L} \exp \times \left[- \int_{\rho_\delta^*(\theta,\phi)}^{\rho_I^*(\theta,\phi)} \alpha_\nu C_{Cl_2} \, d\rho \right] \sin\theta \, d\theta \, d\phi \, d\rho \quad (3)$$

which is valid for monochromatic radiation.

Equation 3 can be integrated analytically for the ρ coordinate; integration along θ and ϕ must be done numerically. The integration limits are rather complex functions of the geometrical characteristics of the lamp-reflector-reactor arrangement. They were derived by Cerdá et al. (1977) and we will write here the final results only (see Figure 2):

$$R_{init} = \frac{2C_{Cl_2}}{4\pi V_L} \int_{\nu=0}^{\nu=\infty} d\nu \Phi_\nu \alpha_\nu E_\nu \Gamma_{Rf,\nu} \Upsilon_{R,\nu} \int_\phi d\phi (r_L^2 - D^2 \sin^2 \xi)^{1/2} \times \int_{\theta_1(\phi)}^{\theta_2(\phi)} d\theta \exp\left[- \int_{\rho_\delta^*(\theta,\phi)}^{\rho_I^*(\theta,\phi)} \alpha_\nu C_{Cl_2} \, d\rho \right] \quad (4)$$

where:

$$\rho_I = \frac{-(hb^2 \cos\phi + ka^2 \sin\phi) + ab[\sigma^2 - (h \sin\phi - k \cos\phi)^2]^{1/2}}{\sigma^2 \sin\theta} \quad (4a)$$

$$\sigma^2 = b^2 \cos^2\phi + a^2 \sin^2\phi \quad (4b)$$

$$h = c + r_I \cos\beta_I \quad (4c)$$

$$k = r_I \sin\beta_I \quad (4d)$$

$$D \sin\xi = -[(x_P + h + c)\sin\phi_E - (y_P + k)\cos\phi_E] \quad (4e)$$

$$D \cos\xi = -[(x_P + h + c)\cos\phi_E + (y_P + k)\sin\phi_E] \quad (4f)$$

$$\phi_E = \tan^{-1}\left[\frac{(m^2 - 1)\sin\phi + 2m\cos\phi}{2m\sin\phi - (m^2 - 1)\cos\phi}\right] \quad (4g)$$

$$m = \frac{a^2(y_P + k)}{b^2(x_P + h)} \quad (4h)$$

$$x_P = \rho_I \sin\theta \cos\phi \quad (4i)$$

$$y_P = \rho_I \sin\theta \sin\phi \quad (4j)$$

The limits for θ are:

$$\theta_{1,2} = \tan^{-1}\left[\frac{\rho_I \sin\theta + D\cos\xi - (r_L^2 - D^2\sin^2\xi)^{1/2}}{1/2(L_R \pm L_L) - z_I}\right] \quad (5)$$

The limits for ϕ must be obtained by solving the following implicit equation:

$$D^2 \sin^2\xi = r_L^2 \quad (6)$$

Clearly, from Eqs. 4a–4j, D and ξ are functions of ϕ; that is:

$$D^2 \sin^2\xi - r_L^2 = f(\phi) \quad (7)$$

Reaction Mechanism: Selection of a Kinetic Scheme

More than forty years ago it was already clearly understood that the absorption of a single photon of light by chlorine molecules leads to chlorine dissociation into atomic species which, in the presence of saturated hydrocarbons, react with them via a chain reaction (Bodenstein and Unger, 1930; Rollefson and Eyring, 1932; Dickinson and Carrico, 1934; Schumacher, 1937; Rollefson, 1938).

In 1956, Gosselain et al. used a general reaction sequence, even though including homogeneous chain-stopping steps only:

$$Cl_2 \xrightarrow{\Phi e^a} 2\,Cl^\bullet \quad \text{(Initiation)} \quad (8a)$$

$$Cl^\bullet + EtH \underset{k_{-2}}{\overset{k_2}{\rightleftharpoons}} ClH + Et^\bullet \quad (8b)$$

$$Cl_2 + Et^\bullet \underset{k_{-3}}{\overset{k_3}{\rightleftharpoons}} ClEt + Cl^\bullet \quad (8c)$$

(Propagation)

$$\left.\begin{aligned} &Cl^{\bullet} + Cl^{\bullet} + M \xrightarrow{k_4} Cl_2 + M && (8d)\\ &Cl^{\bullet} + Et^{\bullet} \xrightarrow{k_5} ClEt && (8e)\\ &Et^{\bullet} + Et^{\bullet} \xrightarrow{k_6} C_4H_{10} && (8f)\end{aligned}\right\} \text{(Homogeneous terminations)}$$

They reported that the kinetic sequence is applicable to thermal or photochemical halogenations of saturated hydrocarbons in homogeneous gas phase or in liquid solutions with nonpolar solvents. They indicated that the mechanism includes all possible reactions within the experimentally explored conditions ($T < 600$ K and low pressures). The heterogeneous terminations were neglected in their proposal because there exist experimental conditions under which they are negligible (high ratio of volume to surface in the reactor; atmospheric or even higher total pressures) and hence they should not be included in a general case.

Noyes and Fowler (1951) indicated that when the atomic chlorine concentration is relatively large (high Cl_2 concentration and high LVREA), the dominant termination step is the atomic chlorine recombination. However, when the concentration of $Cl^{\bullet}$ decreases, a first-order termination step is observed. Two explanations were proposed for this experimental evidence:

1. Bodenstein and Unger (1930) and Kramers and Moignard (1949) assumed that the first-order termination results from atomic chlorine deactivation with some impurity (scavenger of an atomic or free radical species) that is present at an almost constant equilibrium concentration.

2. Another possible mechanism includes deactivation of atomic or free radical species by collisions against the wall. They admitted that under controlled experimental conditions, particularly regarding purity of reactants, this second explanation would be much more plausible.

Regarding this point, since we propose to operate at atmospheric pressure, computational experiments will be performed including the following wall reactions as boundary conditions for the mass conservation equations:

$$\left.\begin{aligned} &Cl^{\bullet} + W \xrightarrow{k_7} \text{Prod.} && (8g)\\ &Et^{\bullet} + W \xrightarrow{k_8} \text{Prod.} && (8h)\end{aligned}\right\} \text{(Heterogeneous terminations)}$$

In addition, following the suggestion of Pritchard et al. (1955) we excluded the reaction on the righthand side of Eq. 8c because its activation energy is much higher than that for the direct reaction. Finally, the true nature of reaction 8f is of no significance for the aims of this work. Be it a disproportionation reaction or a recombination one, for all practical purposes the final products will be almost indistinguishable. Chlorinations are long chain reactions, and products from termination reactions are almost impossible to detect. Hence, for this work we adopted a recombination reaction, Eq. 8f, with the appropriate kinetic parameter.

For simplicity we will use the following notation: Cl_2 (1), $Cl^{\bullet}$ (2), EtH (3), ClEt (4), $Et^{\bullet}$ (5), ClH (6), C_4H_{10} (7), and N_2 (8). Nitrogen will be used as an inert to facilitate the temperature control and the monochloroethane selectivity.

Reactor Modeling

Under the following assumptions:

1. Steady state
2. Streamline, incompressible flow
3. Negligible thermal effects
4. Newtonian fluid with constant physical properties (diffusivities, viscosities, etc.)
5. Angular symmetry
6. Negligible axial diffusion

we can write the mass conservation equations. In dimensionless form, choosing appropriate characteristic scales, they are:

$$\frac{1}{Pe_i Ge}\left(\frac{\partial^2 \Psi_i}{\partial \gamma^2} + \frac{1}{\gamma}\frac{\partial \Psi_i}{\partial \gamma}\right) - U(\gamma)\frac{\partial \Psi_i}{\partial \eta} + \Omega_i = 0 \qquad (9)$$

$$\eta = 0, \forall \gamma \begin{cases} \Psi_1 = \Psi_1^{\circ} = 1 & (9a)\\ \Psi_3 = \Psi_3^{\circ} & (9b)\\ \Psi_i = \Psi_i^{\circ} = 0 \quad (i = 2, 4\text{–}7) & (9c)\end{cases}$$

$$\forall \eta, \gamma = 0 \left\{ \frac{\partial \Psi_i}{\partial \gamma} = 0 \right. \qquad (9d)$$

$$\forall \eta, \gamma = 1 \begin{cases} \dfrac{\partial \Psi_j}{\partial \gamma} = 0 & (9e)\\ \dfrac{\partial \Psi_\ell}{\partial \gamma} = -Pe_\ell \Omega_{w,\ell} & (9f)\end{cases}$$

in which j stands for stable species (j = 1, 3, 4, 6, and 7), ℓ denotes atomic or free radical species, and $\Omega_{w,\ell}$ is the rate of heterogeneous termination for species ℓ, (ℓ = 2 and 5).

We will see further ahead that the boundary condition of Eq. 9f can be simplified for this system without losing accuracy in the final results.

The geometric number Ge($Ge = r_R/L_R$), is an important number in photoreactor analysis. Not only does it affect the Peclet number, it also has a strong influence on the optical thickness of the reactor.

In Eqs. 9 and 9f we defined:

$$\Omega_i = \frac{R_i L_R}{\langle v \rangle C_1^{\circ}} \qquad (10)$$

and

$$\Omega_{w,\ell} = \frac{R_{w,\ell}}{\langle v \rangle C_1^{\circ}} \qquad (11)$$

which have the following dimensionless expressions:

$$\Omega_1 = -J - K_3 \Psi_1 \Psi_5 + K_4 \Psi_2^2 \Psi_8 \qquad (12)$$

$$\Omega_2 = 2J - K_2 \Psi_2 \Psi_3 + K_{-2} \Psi_5 \Psi_6 + K_3 \Psi_1 \Psi_5 - 2K_4 \Psi_2^2 \Psi_8 - K_5 \Psi_2 \Psi_5 \qquad (13)$$

$$\Omega_3 = -K_2 \Psi_2 \Psi_3 + K_{-2} \Psi_5 \Psi_6 \qquad (14)$$

$$\Omega_4 = K_3 \Psi_1 \Psi_5 + K_5 \Psi_2 \Psi_5 \qquad (15)$$

$$\Omega_5 = K_2\Psi_2\Psi_3 - K_{-2}\Psi_5\Psi_6 - k_3\Psi_1\Psi_5 - K_5\Psi_2\Psi_5 - 2K_6\Psi_5^2 \quad (16)$$

$$\Omega_6 = K_2\Psi_2\Psi_3 - K_{-2}\Psi_5\Psi_6 \quad (17)$$

$$\Omega_7 = K_6\Psi_5^2 \quad (18)$$

$$\Omega_{w,2} = K_7\Psi_2 \quad (19)$$

$$\Omega_{w,5} = K_8\Psi_5 \quad (20)$$

In all these equations, the following additional definitions were used:

$$J = \frac{R_{init}L_R}{\langle v\rangle C_1^\circ} \quad (21)$$

$$K_r = \frac{k_r L_R C_1^\circ}{\langle v\rangle}, \quad r = 2, -2, 3, 5, \text{and } 6 \quad (22)$$

$$K_r = \frac{k_r L_R C_1^{\circ 2}}{\langle v\rangle}, \quad r = 4 \quad (23)$$

$$K_r = \frac{k_r}{\langle v\rangle}, \quad r = 7 \text{ and } 8 \quad (24)$$

The reactor model and the radiation field model are now completely described by Eqs. 4 to 7 and 9 to 24. We still have to deal with the existence of polychromatic radiation and the explicit form of e^a.

Description of the System

The photoreactor model shows a strong dependence on the geometrical characteristics and optical properties of the system (reactor, reflector, and lamp), as well as the radiation spectral distribution of absorption by reactants, emission by the source, absorption by the reactor wall, and reflection by the "elliptical mirror."

For all the preliminary studies and computations, the following conditions were adopted:

- Chlorine absorptivities were taken from the original data by Gibson and Bayliss (1933) and recalculated by Cassano (1968); they agree very well with values reported by Calvert and Pitts (1966). Absorption by ethyl chloride need not to be accounted for since it is only significant at wavelengths shorter than those used in this work (below 2,300 Å).
- The radiation source output power was taken as a nominal 100 W, using the spectral distribution of a commercial lamp provided by Hanovia (Hanovia SOL 608 A).
- The geometrical characteristics of the reactor, reflector, and radiation source are listed in Table 1. Since $e = 0.4$ and $r_R/r_L = 0.33$, the conditions found by De Bernardez and Cassano (1982) to safely neglect angular asymmetries are satisfied.
- The physical properties were obtained as follows:

(i) Densities and viscosities were calculated by a linear combination of the properties of the pure components using composition as a weighting factor; given the excess of nitrogen further refinements would have been unjustified.

(ii) Molecular diffusivities were calculated considering that the system will be tested under excess of an inert (N_2). Following Reid et al. (1977) we used the empirical correlation of Fuller et al. (1966). For the buthane-nitrogen and ethane-nitrogen mixtures we used the experimental data published by Boyd et al. (1951).

Table 1. Geometrical Characteristics of Reactor, Reflector, and Lamp

r_R, cylindrical radial coordinate of reactor	0.2 cm
L_R, length of reactor	10 cm
r_L, cylindrical radial coordinate of lamp	0.6 cm
L_L, length of lamp	12 cm
L_{Rf}, length of reflector	40 cm
a, ellipse semimajor axis	53.5 cm
c, half-distance between focuses	21.4 cm
e, ellipse eccentricity	0.4

- Kinetic constants were taken from well-established published data; they are included in Table 2. When more than one source of information was available we found excellent agreement among data from different laboratories. The only exception was the value of k_4, and we adopted $k_4 = 2 \times 10^{16}$ (cm^3)^2/mol^2 · s according to Ayscough et al. (1962), Hutton and Wright (1965), and Clyne and Stedman (1968). An experimental value on Pyrex glass was used for k_7 (Hutton and Wright, 1965; Clyne and Stedman, 1968). On the other hand, considering that the collision efficiencies for different radicals and atoms are similar (Noyes and Fowler, 1951), k_8 was assumed to have the same order of magnitude.
- The primary quantum yield needs a more careful analysis. Our model requires its numerical value and, for the general case, its wavelength dependence. Consequently we must look into the primary process. Generally, the absorption of light by diatomic molecules results in the dissociation of the absorbing molecule into two atomic species. Under these conditions, resorting to the primary quantum yield as it was defined by Noyes and Leighton (1941), we have:

$$\Phi_\nu = \frac{\text{number of molecules dissociated by the primary process}}{\text{number of quanta of frequency } \nu \text{ absorbed by the molecule}} \quad (25)$$

After absorption of radiation, the primary process has the following possibilities:

$$Cl_2^* \rightarrow 2Cl^\bullet \quad \text{spontaneous dissociation} \quad (P1)$$

Table 2. Kinetic Constants

Constant	Value	Refs.*
k_2	4.03 10^{13} cm^3/mol · s	b, c, e, i, j
k_{-2}	2.18 10^6 cm^3/mol · s	b
k_3	2.34 10^{12} cm^3/mol · s	b
k_{-3}	2.99 10^{-2} cm^3/mol · s	b
k_4	2.00 10^{16} (cm^3)^2/mol^2 · s	a, b, d, f
k_5	2.00 10^{14} cm^3/mol · s	b
k_6	3.16 10^{13} cm^3/mol · s	g, h, k
k_7	0.5 cm/s	d, f

*a. Ayscough et al. (1962), b. Chiltz et al. (1963), c. Clark & Clyne (1970), d. Clyne & Stedman (1968), e. Davis et al. (1970), f. Hutton & Wright (1965), g. Ivin & Steacie (1951), Ivin et al. (1952), h. Kerr & Trotman-Dickenson (1960), i. Knox & Nelson (1959), j. Pritchard et al. (1955), k. Steacie (1954)

$$Cl_2^* \rightarrow Cl_2 + h\nu \quad \text{fluorescence} \tag{P2}$$

$$Cl_2^* + M \rightarrow 2Cl^* + M$$

dissociation induced by collisions (P3)

$$Cl_2^* + M \rightarrow Cl_2 + M \quad \text{deactivation by collisions} \tag{P4}$$

$$Cl_2^* + W \rightarrow Cl_2 + W \quad \text{deactivation by wall collisions} \tag{P5}$$

$$Cl_2^* + A \rightarrow \text{Products} \quad \text{reaction with other molecules} \tag{P6}$$

By inspection of the potential energy curves for the Cl_2 molecule (Herzberg, 1950) it can be concluded that Cl_2^* is very unstable and immediately dissociates into two atomic species. Thus, reaction P1 will be the dominant process with the only possible exception of P3. Since both produce the same product, it can safely be assumed that $\Phi_\nu = 1$. This behavior occurs along the total range of continuous absorption by chlorine. Therefore the result can immediately be extended and we can choose $\Phi = 1$ regardless of the wavelength. In support of this, it should be noted that Chiltz et al. (1963) observed no variation in the primary quantum yield for chlorine dissociation, adding more evidence to the hypothesis of adopting $\Phi = 1$. Under these circumstances, when using polychromatic light in our photochlorinations we can safely neglect spectral variations in the primary quantum yield. However, the lamp output power and the absorption by chlorine are wavelength-dependent. A deeper analysis shows that the wavelength dependence of Γ_{Rf} and Υ_R must also be included. Average values provided by the quartz manufacturer indicated that for the wavelength range of interest, $\Upsilon_R \neq \Upsilon_R(\nu)$ (Heraeus Quarzchmelze *Tech. Bull.*). On the other hand the values of $\Gamma_{Rf,\nu}$ were incorporated in the model equations.

Polychromatic Radiation

The dimensionless form of the LVREA is:

$$J = \frac{R_{init} L_R}{\langle v \rangle C_1^\circ} = \frac{2\Phi L_R \langle \Upsilon_R \rangle}{4\pi V_L \langle v \rangle} \Psi_1 \int_{\nu=0}^{\nu=\infty} d\nu \Gamma_{Rf,\nu} E_\nu \alpha_\nu \times \int_\phi d\phi (r_L^2 - D^2 \sin^2 \xi)^{1/2} \times \int_{\theta_1(\phi)}^{\theta_2(\phi)} d\theta \exp\left[- \int_{\rho_\sigma^*(\theta,\phi)}^{\rho_f^*(\theta,\phi)} \alpha_\nu C_1 \, d\rho' \right] \tag{26}$$

Let us concentrate on the frequency integral. It can be written as:

$$I = \int_{\nu=0}^{\nu=\infty} d\nu \Gamma_{Rf,\nu} E_\nu \alpha_\nu \exp\left[- \int_{\rho_\sigma^*(\theta,\phi)}^{\rho_f^*(\theta,\phi)} \alpha_\nu C_1 \, d\rho' \right] \tag{27}$$

The range of appreciable continuous absorption by chlorine covers from $\lambda_1 = 2{,}500$ Å to $\lambda_2 = 5{,}000$ Å (Herzberg, 1950); the reflector is effective between $\lambda_1' = 1600$ Å and $\lambda_2' \rightarrow \infty$ (Sylvania *Tech. Bull.*); the lamp emission is significant from $\lambda_1'' = 2{,}200$ Å to $\lambda_2'' = 14{,}000$ Å (Hanovia, 1959).

Hence, chlorine absorption puts much closer bounds to the frequency integral. It can be rewritten as:

$$I = \int_{\lambda_1}^{\lambda_2} d\lambda \Gamma_{Rf\lambda} E_\lambda \alpha_\lambda \exp\left[- \int_{\rho_\sigma^*(\theta,\phi)}^{\rho_f^*(\theta,\phi)} \alpha_\lambda C_1 \, d\rho' \right] \tag{28}$$

For the most general case λ_1 is defined by the lower practical bound of the primary quantum yield, lamp emission, reactant (or product) absorption, reactor wall transmission, and reflector reflectivity, whichever is largest. Similarly, λ_2 is defined by the upper practical bound of the same properties, whichever is shortest. In practice, $\Gamma_{Rf\lambda}$ for aluminum sheets of the specular type and α_λ for chlorine, are continuous functions of λ. On the other hand, most UV lamps provide an emission spectrum that is discontinuous. Let us write:

$$E_\lambda = E_\sigma \delta(\lambda - \lambda_\sigma) \tag{29}$$

with δ being the Dirac function. We can now substitute for the polychromatic lamp a finite number of monochromatic lamps, each emitting the output power corresponding to each line of emission E_σ. The interval of the lamp emission lines for this particular case is wider than the one corresponding to absorption by chlorine. Hence λ_1 and λ_2 can remain as the lower and upper bounds for I. Then Eq. 28 can be written as:

$$I = \sum_{\sigma=1}^{\sigma=n} \int_{\lambda_1}^{\lambda_2} d\lambda E_\sigma \delta(\lambda - \lambda_\sigma) \alpha_\sigma \Gamma_{Rf,\sigma} \times \exp\left[- \int_{\rho_\sigma^*(\theta,\phi)}^{\rho_f^*(\theta,\phi)} \alpha_\sigma C_1 \, d\rho' \right] \tag{30}$$

$$I = \sum_{\sigma=1}^{\sigma=n} E_\sigma \alpha_\sigma \Gamma_{Rf,\sigma} \exp\left[- \int_{\rho_\sigma^*(\theta,\phi)}^{\rho_f^*(\theta,\phi)} \alpha_\sigma C_1 \, d\rho' \right] \tag{31}$$

The summation must be performed over all the spectral lines of the lamp emission spectrum for which $\alpha_\sigma \neq 0$ and $\Gamma_{Rf,\sigma} \neq 0$. Here, E_σ is the lamp output power at $\lambda = \lambda_\sigma$; α_σ is the absorption coefficient of chlorine at $\lambda = \lambda_\sigma$; $\Gamma_{Rf,\sigma}$ is the reflection coefficient at $\lambda = \lambda_\sigma$; and n is the number of emission lines produced by the lamp between λ_1 and λ_2.

With the following definitions:

$$\epsilon = \frac{D \sin \xi}{r_L} \tag{32}$$

$$K_{1\sigma} = \frac{\Phi E_\sigma \alpha_\sigma \Gamma_{Rf,\sigma} L_R}{4\pi^2 \langle v \rangle r_L L_L} \tag{33}$$

$$\Lambda_\sigma = \alpha_\sigma C_1^\circ r_R \tag{34}$$

$$\Delta = \rho^* / r_R \tag{35}$$

Eq. 26 is finally written in dimensionless form as:

$$J = 2\langle T_R \rangle \Psi_1 \int_\phi d\phi (1 - \epsilon^2)^{1/2} \int_{\theta_1(\phi)}^{\theta_2(\phi)} d\theta \times \sum_{\sigma=1}^{\sigma=n} K_{1\sigma} \exp\left[- \Lambda_\sigma \int_{\Delta_\sigma(\theta,\phi)}^{\Delta_f(\theta,\phi)} \Psi_1 \, d\Delta' \right] \tag{36}$$

Equation 36 must be substituted into Eqs. 12 and 13. It clearly establishes two important features of a photochemical reactor:

1. The reaction rate terms are coupled with an energy bal-

ance (radiation balance) even for isothermal conditions. This coupling is transferred into the system of partial differential equations. Since the attenuation is mathematically expressed through an integral, every photochemical reactor must be modeled by integro-differential equations.

2. The radiation source is an inseparable part of photoreactor modeling. In fact the shape (r_L, L_L) as well as the total (E) and spectral distribution (E_o) output power, go into the system of differential equations governing the process. Moreover, they are part of key dimensionless numbers.

Simplifications; Final Model Equations

Two aspects can be further analyzed in order to achieve a simpler mathematical modeling. We will look at the problem of wall reactions and at the possibility of applying the microsteady-state approximation (MSSA) locally.

To do so we will solve the system of partial integro-differential equations (PIDE's) under the following conditions:

1. With wall reactions
2. Without wall reactions
3. With the full set of PIDE's
4. With the MSSA.

To solve the equations we are faced with the following difficulties: the LVREA is not only a point function of position [$e^a = e^a(r_I, \beta_I, z_I,$ parameters)], but is also a functional of all the optical properties of the space through which every ray reaching point I has traveled. This is illustrated by Figure 3a. As a consequence, there exists a very close association between the extent of the reaction in the whole reactor (which controls the concentration of the reactant absorbing species) and the absorption rate at each point; that is, to know the reaction rate at each point I we must know the value of $|q_v|_I$ at that point, which in turn depends on the concentration of the absorbing species along the trajectory of every ray reaching point I from the whole reaction volume; at the same time, in order to know the concentration of the absorbing species at each point in the reaction volume we need to know the reaction extent at every point. (Or what is the same, the reaction rate at every point). Therefore, in order to solve this cyclic link extent-of-reaction/attenuation-of-radiation, an iterative procedure must be superimposed on the numerical technique used to solve the system of PIDE's. Starting from an initial value of concentration, for instance $\Psi_1 = 1$ in the whole reactor, one must solve the problem until an essentially steady state concentration of reactants is achieved. This is done by sweeping the finite-difference mesh as many times as needed until an acceptable, prescribed minimum error is attained.

This is only part of the problem because the attenuation phenomenon is a three-dimensional process, Figure 3b; with the hypothesis of angular symmetry, the mass balances are bidimensional. Without loss of rigor, the problem can be solved by using a cylindrical projection of all concentration values on the rectangular mesh used in the numerical solution, Figure 3b. This approach was initially suggested by Romero et al. (1983) for an annular reactor. The extension to reflected radiation is only a matter of a more complex algebra.

The problem was numerically solved with a Digital-Vax 11/780 computer with 2 Mbyte core memory and 200 Mbyte disk memory, thus making the work expedient. The Vax was used on a time-sharing basis (20 terminals), and the time for each run (calculation of the average outlet conversion at one given operating condition) took, on the average, about 30 min.

Wall reaction effects

Figure 4 shows radial profiles for atomic chlorine obtained with the boundary conditions given by Eqs. 9e and 9f for stable and atomic or free radical species, respectively. It is seen that close to the reactor wall there is a small effect. However, no appreciable changes in the concentration profiles for stable molecules were observed when the results were compared with those obtained using boundary condition Eq. 9e for all species, including $i = 2$ and $i = 5$.

Table 3 shows the average exit conversion for stable species with and without wall reactions. These values were computed

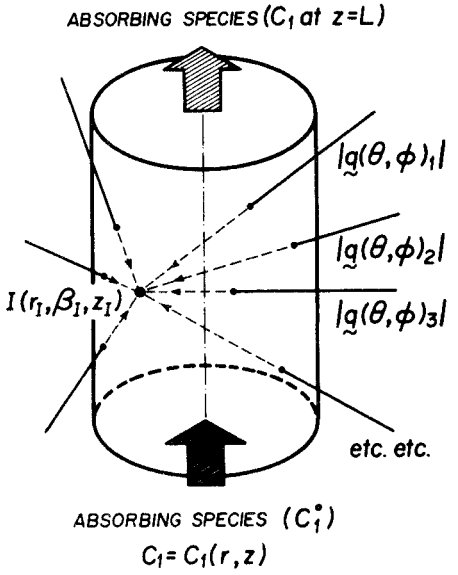

Figure 3a. Representation of coupling attenuation-of-radiation/extent-of-reaction.

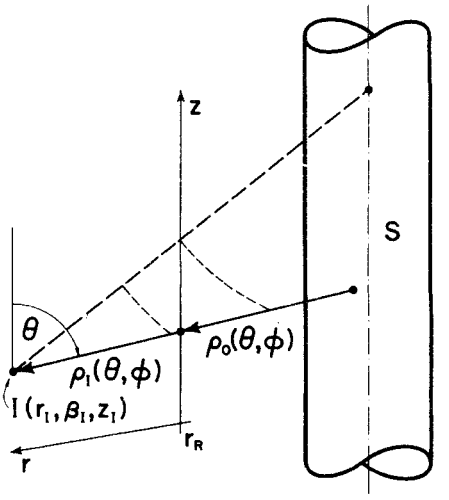

Figure 3b. Cylindrical projection incorporating three-dimensional attenuation of radiation into two-dimensional mass balances.

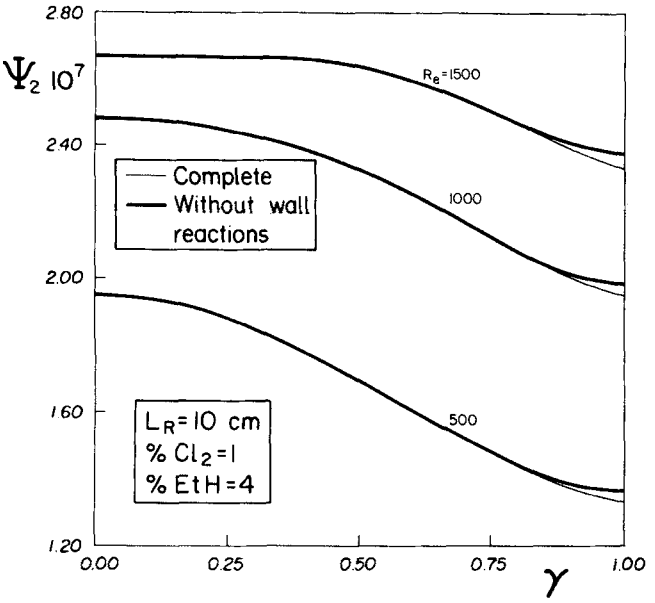

Figure 4. Atomic chlorine radial concentration profiles with and without wall reactions.

according to:

$$\langle \Psi_i \rangle = \frac{\int_A U(\gamma)\Psi_i(\gamma, 1)\gamma \, d\gamma d\theta}{\int_A U(\gamma)\gamma \, d\gamma d\theta} = 4\int_0^1 (1-\gamma^2)\Psi_i(\gamma, 1)\gamma \, d\gamma \quad (37)$$

and

$$X = 1 - \langle \Psi_1 \rangle \quad (38)$$

It is clear that wall reactions have no influence on the reactor modeling, at least for this particular kinetic system. Since the ratio of reactor surface to reactor volume is rather large for this case ($2/r_R$ with $r_R = 0.2$ cm), we may conclude that for all practical purposes, at atmospheric pressure (or higher pressures) they can surely be neglected. The reason is that a commercial-scale reactor will have a ratio of A_R to V_R always smaller than the one used here, perhaps up to two orders of magnitude smaller. Consequently, we have excluded reactions 8g and 8h. This means that all reactor walls were considered nonpermeable and boundary condition Eq. 9e can be used for $i = 1$ to 7.

Table 3. Average Exit Conversions

	X, %			
Re	Exact	W/out Wall Reactions	MSSA	$\frac{X_{exact} - X_{SS}}{X_{exact}} \cdot 100$
500	43.74	43.79	44.71	2.2
1,000	25.35	25.40	26.65	5.1
1,200	22.25	22.29	23.44	5.4
1,500	14.94	14.97	16.01	7.2

Microsteady-state approximation

In a photoreactor with practical optical thickness, nonuniform radiation energy flux density profiles are unavoidable. Hence, concentration nonuniformities are always present. Thus, mass fluxes will also be present. Unless the experiments are carried out in a well-stirred reactor we cannot apply the steady state hypothesis for the whole reactor but only locally. This procedure can be applied to short-lived intermediates such as Cl$^\bullet$ and Et$^\bullet$. Locally, it implies that:

$$\Omega_i = 0 \quad \text{for} \quad i = 2 \text{ and } 5 \quad (39)$$

For these two species we must then solve only algebraic equations. They remain coupled to the remaining PIDE's through the reaction rate terms where concentrations of atomic chlorine or ethyl radicals are involved. Equation 39 has the following form:

$$2K_4\Psi_3\Psi_2^2 + (K_2\Psi_3 + K_5\Psi_5)\Psi_2 - (2J + K_{-2}\Psi_5\Psi_6 + K_3\Psi_1\Psi_5) = 0 \quad (40)$$

$$2K_6\Psi_5^2 + (K_{-2}\Psi_6 + K_3\Psi_1 + K_5\Psi_2)\Psi_5 - K_2\Psi_2\Psi_3 = 0 \quad (41)$$

With the MSSA we can reduce the modeling of the monophotochlorination of ethane to a system of five parabolic PIDE's (with the appropriate initial and boundary conditions), coupled to two algebraic equations for the unstable intermediate species. The system was solved with Eq. 9 with Eqs. 9a to 9e (valid for $i = 1$ to 7), Eqs. 12 to 18, and Eq. 36. The results were compared substituting Eqs. 40 and 41 for the PIDE's for $i = 2$ and 5.

Figure 5 shows atomic chlorine axial concentration profiles for $\gamma = 0$ using Re as a parameter. Recalling the order of magnitude of these concentrations (10^{-12} to 10^{-13} mol/cm^3), it is clear that the MSSA holds. The most unfavorable condition was found for higher Re (Re = 1,500).

The plot shows significant difference when $\eta \to 0$, which is what we might have expected since reactants must spend some

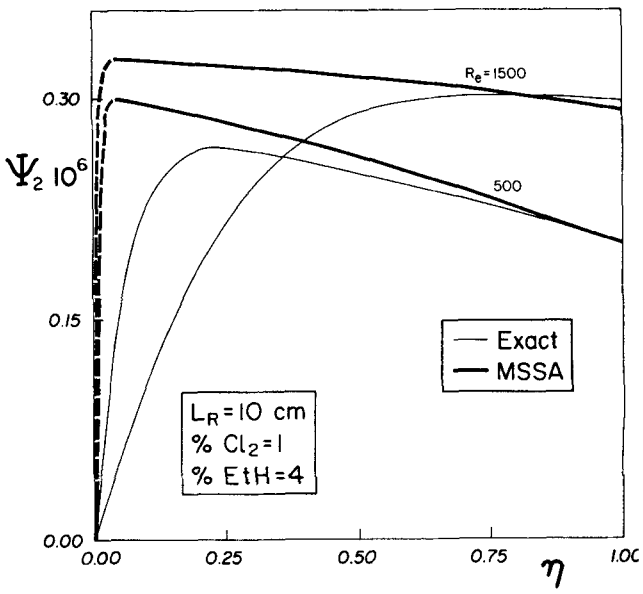

Figure 5. Atomic chlorine axial concentration profiles with and without local MSSA.

time inside the reactor to achieve the "near-constant" concentration of intermediates. It is also seen that the MSSA hypothesis is only a very good approximation and that in fact, in the axial direction, intermediate species follow a pattern of behavior close to that corresponding to the stable species from which they originated ($Cl^\bullet$ with Cl_2 and $Et^\bullet$ with EtH). (This is not the case for radial concentration profiles of atomic chlorine, as will be seen.) To compare the quality of the MSSA we may compute:

$$t_{SS} = \frac{\eta_{SS} L_R}{\langle v \rangle} \tag{42}$$

where t_{SS} is the mean residence time needed to reach a quasi steady-state concentration for an intermediate species and η_{SS} the value of the axial coordinate where it is achieved. The longer the value of t_{SS}, the poorer the approximation. When Re is large due to a large value of $\langle v \rangle$, η_{SS} must also be large since L_R is fixed and t_{SS} is constant for a given reaction and a given value of the radiation field. Hence for large values of $\langle v \rangle$ the MSSA will deviate appreciably from the exact results. In this case, a large fraction of the total reactor length will be calculated with an assumption that is not adequate, not even as a good first approximation. For these cases, under extremely unfavorable conditions η_{SS} may represent more than 50% of the reactor length. Let us indicate here that we have never gone to Re larger than 1,500 in order to make sure that the laminar flow is maintained. Under this restriction, molecular properties have a very precise meaning. (Nitrogen concentration was always larger than 80% in order to work within a range of concentrations where the values of D_{im} may be estimated as pseudobinary mixtures). All this discussion regarding $Cl^\bullet$ also holds for $Et^\bullet$.

For practical applications, it is important to know how much the average exit concentration of a key compound (some stable species) differs when it is calculated with the exact solution and when the MSSA is used. Results for different values of Re (by changing only $\langle v \rangle$) are shown in Table 3. These results indicate that even under the most unfavorable conditions (higher values of Re), the error is never larger than 8%. Consequently, the MSSA can be incorporated to the reactor modeling, considerably reducing the complexity of the problem. This will be even more significant if the reacting system operates at high chlorine concentrations and conversions. Then, di- and trichlorinated compounds will appear and the reaction mechanism will involve a larger number of species and steps.

However, we may keep in mind that an additional simplification could have been used. In long chain radical reactions as in our case, the long-chain approximation (Gavalas, 1966), can be used since under most operating conditions initiation and termination steps will be negligible in comparison with propagation steps. We did not resort to it because it does not simplify the problem drastically once the kinetic microsteady-state approximation has been used. The bottleneck clearly lies in the prediction of the radiation field and in the solution of the coupling attenuation-of-radiation/extent-of-reaction described at the beginning of this section.

For a value of $\eta = 0.5$, Figure 6 shows atomic chlorine radial concentration profiles. The influence of the parabolic velocity profile superimposed on the radiation field is clear.

Having reached a reasonable degree of simplification in our model, we can proceed with a description of the experimental verifications.

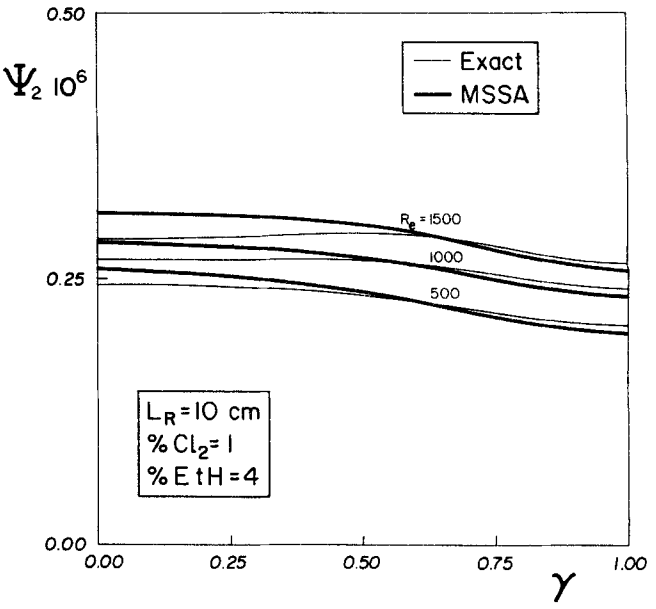

Figure 6. Atomic chlorine radial concentration profiles with and without local MSSA.

Experimental Method

Setup

Figure 7 shows a schematic flow sheet of the experimental apparatus.

The feed gas contains:

- Nitrogen: La Oxigena, 99.998%. Purified by four absorbers, three containing $Na_2S_2O_4$ solution and one concentrated H_2SO_4. They were in line with traps for liquid drops. The flow was measured and controlled with a Matheson mass flow rate meter that was previously calibrated against a wet test meter.
- Ethane: Matheson, C.P. grade, 99.0%. Although no detectable O_2 was found in the feed, it was purified by two absorbers containing $Na_2S_2O_4$ solution and concentrated H_2SO_4, respectively, which were followed by liquid drop traps. The ethane flow rate was measured with a Matheson mass flow meter calibrated against a bubble flow meter.
- Chlorine: Matheson, H.P. grade, 99.5%, was dried with concentrated H_2SO_4 (a second flask was used to eliminate liquid drops) and then condensed in a Monel Metal gas cylinder at 70 KPa and -60°C. Then it was vented to eliminate any noncondensable gases. Its volume was chosen so as to contain enough liquid chlorine to permit 10 h of normal operation. After reaching ambient temperature, the small cylinder was connected to the chlorine feed tube in the system. The chlorine flow rate was measured with a Matheson mass flow meter calibrated by chemical absorption followed by chemical analysis.

All parts in contact with chlorine or the reacting mixture were made of glass, quartz, Teflon, or Monel Metal. All pipes were exclusively made of Pyrex glass or Teflon. Teflon Swagelok fittings were used in all connections. The reactor was made of quartz Suprasil quality, with 0.4 cm ID and 0.625 cm OD. Two nominal reactor lengths were used, L_{R1} = 12 cm and L_{R2} = 30 cm. Since the reactor tube must be cleaned very often and positioning at the focal axis of the ellipse is very critical, a special device was constructed. It consisted in a holding support having three arms controlled by micrometric screws, symmetrically

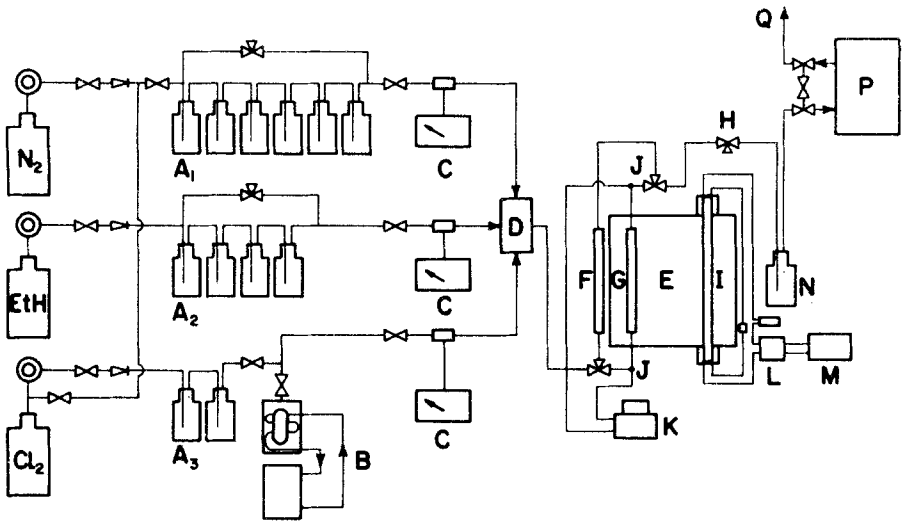

Figure 7. Flow sheet of experimental setup.

A_1, A_2, A_3. Nitrogen, ethane, chlorine purification absorbers
B. Distillation system for chlorine purification
C. Mass flow rate flowmeters and controllers
D. Mixer
E. Elliptical reflector
F. Dark reactor
G. Quartz reactor
H. Chlorine gas sampling
I. Tubular radiation source
J. Pt resistance thermometers
K. Digital temperature meter
L. Voltage regulator
M. Lamp operating intensity, voltage, and input power meter
N. Chlorine gas absorber
P. Gas sampling loop for GC analysis
Q. vent

separated 2.09 rad (120°) from each other. The lamp was a General Electric G30T8 (Germicidal) with 30 W nominal input power. Its dimensions were $L_L = 81.3$ cm and $r_L = 1.27$ cm. Its operation was continuously monitored (intensity, voltage, and input power) and its input voltage was constantly controlled to ensure that 30 W were always fed to the lamp. A germicidal lamp is not the best choice for a chlorination reaction; it emits 95% of its output power in the far UV range, with almost 90% of it at 2,537 Å. Absorption by chlorine has a maximum at 3,300 Å. Hence, other radiation sources may have a much better energy yield. However, the G30T8 source was the best choice in order to have a low-energy, nonfluorescent arc lamp with the length and diameter required for a suitable verification of the radiation and reactor model (De Bernardez and Cassano, 1982). In accordance with the manufacturing specifications, the lamp was always used after a minimum of 100 h of operation to make sure that it was used during the most stable period of its average lifetime. Provisions were taken to ensure the proper operation of the lamp according to its nominal output power. The reflector was made of aluminum sheet, specularly finished with Alzac treatment. Its dimensions were $L_{Rf} = 59$ cm, $a = 53.5$ cm, $e = 0.4$. It was constructed within less than 0.05 cm tolerance. With the exception of the irradiated length of the reactor, all other parts of the system were blackened to avoid any possible effect produced by laboratory light. An additional tube (dark reactor) with the same hydrodynamic characteristics as the one made of quartz was placed in a bypass position to improve the control of the steady state operation and to check for the dark reactions.

Procedure

After setting flow rates, 2 h were allowed for stabilization. The chlorine in the feed was always checked by chemical absorption and iodine titration. This was also done to verify the stability of the chlorine mass flow rate calibrations. For every operating condition, the absence of dark reactions was checked in the dark reactor. After the lamp was turned on, all the operating parameters were allowed to reach their steady state values (about 30 min). Then all measurements were repeated. In all cases, they included feed and product stream concentrations by chemical absorption (Cl_2) and gas chromatography (ethane when the lamp was off, ethane and chlorinated compounds when the lamp was on). To avoid corrosion of the gas chromatograph (GC), the exit stream was always passed through a NaOH aqueous solution and a water absorber. The GC gas sampling loop could be placed in the sampling stream whenever it was needed. The Cl_2 and GC analyses were repeated until steady state conversions were obtained. Every 45 min an analysis was made (Cl_2, C_2H_6, and chlorinated compounds). After three consecutive analyses showed that the steady state had definitely been achieved, the run was concluded. Every experimental point obtained with this procedure required about 8 h of operation.

Once the run was completed, the lamp was turned off and the entire system was washed with N_2 for several hours. Then the reactor was removed and cleaned with carbon tetrachloride, KOH alcoholic solution, distilled water, and finally absolute ethanol. It was finally dried with dry air and positioned again at the focal axis of the reflector.

Temperature was carefully controlled at the inlet and outlet reactor ends. When the chlorine conversion was lower than 50%, temperature differences were never larger than 2°C. Beyond 50% conversion temperature differences as large as 5°C were observed.

The dark reactions were found to be negligible and the observed values were always smaller than the experimental error.

The experimental exit conversion defined as:

$$X_{exp} = 1 - \frac{C^e_{Cl_2}}{C^o_{Cl_2}} \tag{43}$$

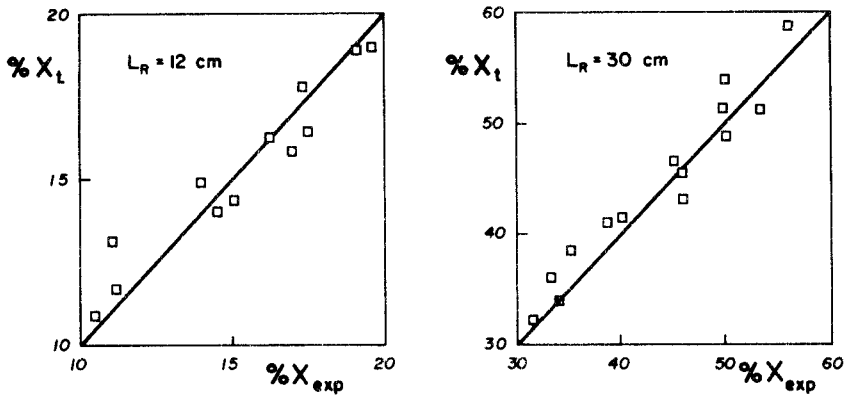

Figure 8. Compendium of experimental results.

was compared with results computed by means of:

$$X_t = 1 - \langle \Psi_{Cl_2} \rangle \tag{44}$$

with $\langle \Psi_i \rangle$ calculated according to Eq. 37.

Results

Figures 8a and 8b give a compendium of the experimental results for the L_{R1} and L_{R2} reactors, respectively. The chlorine mole fraction was changed between 0.5 and 7%, ethane between 0.5 and 14%. Nitrogen always provided the make-up gas to achieve atmospheric pressure. The Reynolds number was maintained near 650 and the nominal temperature was always kept at 25°C. For the small reactor, the chlorine conversion was below 20%; for the large reactor it reached values up to 60%. Under no conditions were differences between predicted and experimental values greater than 15%. Only at very high conversions were dichlorinated compounds (1,1 ethane dichloride and 1,2 ethane dichloride) observed in the GC analysis, and the amounts were negligible. It should be recalled that we always worked under excess of ethane and low chlorine mole fraction in the feed.

Figures 9a and 9b (for L_{R1} and L_{R2}, respectively) show predicted (solid line) and experimental values. From these, the effect of the chlorine mole fraction in the feed on the average exit chlorine conversion can be analyzed. Figures 10a and 10b show the effect of the mole fraction of ethane on the product yield. Volumetrically averaged exit conversions were again used.

All the experimental results show extremely good agreement with the theoretical predictions. It is interesting to remark that the total mass balance was also experimentally verified within a 3% error, satisfying:

$$C^o_{Cl_2} = C^e_{Cl_2} + C^e_{ClEt} \tag{45}$$

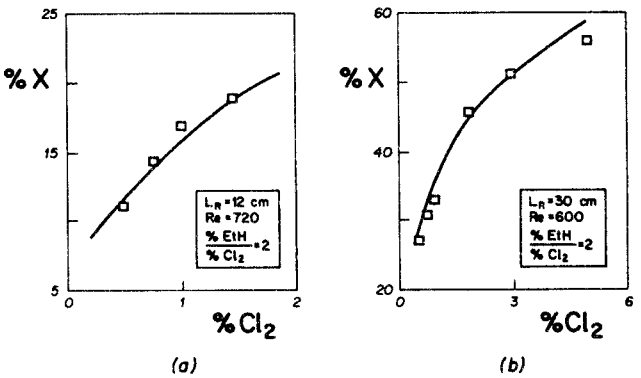

Figure 9. Effect of chlorine mole fraction on average chlorine exit conversion.
— predicted; □ experiment

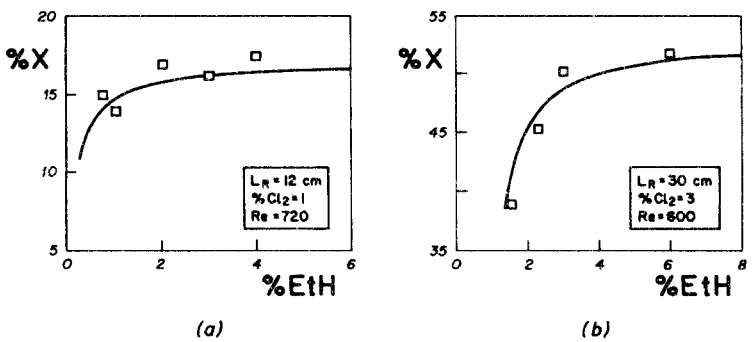

Figure 10. Effect of ethane mole fraction on average chlorine exit conversion.
— predicted; □ experiment

and

$$C^{o}_{EtH} = C^{e}_{EtH} + C^{e}_{ClEt} \qquad (46)$$

simultaneously.

The agreement suggests two important conclusions:

1. The microkinetic constants reported in the literature are very good for reactor design purposes
2. The proposed radiation and reactor models provide a reliable design method

As an additional result, Figure 11 shows clear evidence of the inability of the present-day formulation of linear models to predict the experimental values when curved reflecting surfaces are part of the radiation emitting system. This is a common problem when a tubular lamp (if it is modeled as a line) is placed parallel to the straight line that generates the cylindrical reflector. Previously, this result had been found experimentally in a different emission system by Alfano et al. (1984), performing measurements with a thermopile, and by Clariá (1984) for the case of an actinometric reaction. The experimental points can be interpreted satisfactorily only by a model that includes the curvature of the cylindrical tubular lamp as a parameter in the modeling equations.

Therefore, since the model has shown its ability to predict the reactor performance, we can proceed further with a detailed parametric analysis, using computer simulation experiments.

Parametric Study

Choice of radiation source

This is one of the best choices among operating variables to be manipulated in order to improve yield. Let us compare conversions obtained with the G30T8 lamp and another radiation source with the same power consumption but with a different spectral distribution of the output power. As an idealization let us assume that a lamp concentrates all its emission at 3,300 Å, all geometrical characteristics remaining the same. This would be the ideal lamp for optically thin chlorinations, particularly to obtain monochlorinated derivatives when very low proportions of chlorine must be used. Figure 12 shows the predicted results.

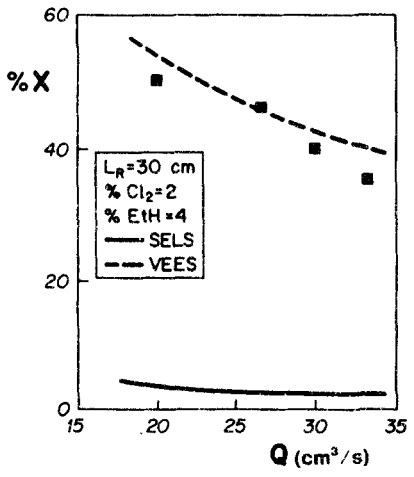

Figure 11. Prediction inability of linear models when used in combination with curved reflecting surfaces.

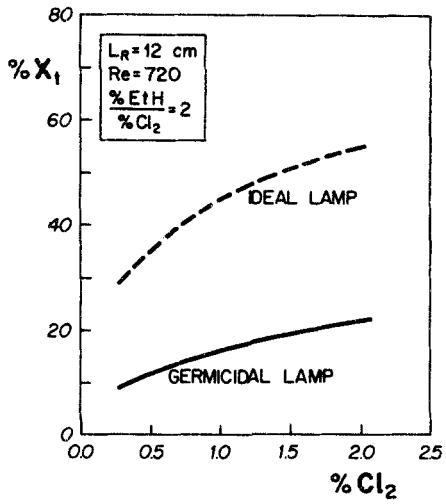

Figure 12. Comparison of conversions obtained using germicidal lamp and "ideal" lamp.

With the same power consumption, conversions can be tripled. This shows that the design of a photoreactor is a combination of reactor analysis with an appropriate choice (or design) of the radiation source.

Concentration profiles

Here we present the computer simulation results obtained under the conditions given earlier in the system description section. Stable species, (excluding some negligible concentrations of radical-radical homogeneous recombinations that are not relevant for this study) as well as atomic and free radical intermediates will be discussed. In all the computer runs, the Reynolds number was kept below 1,500 in order to have laminar flow and to make sure that the adopted velocity profile and the molecular properties (such as viscosity and diffusivities) are well-defined quantities.

Figure 13 shows axial profiles for atomic and molecular chlo-

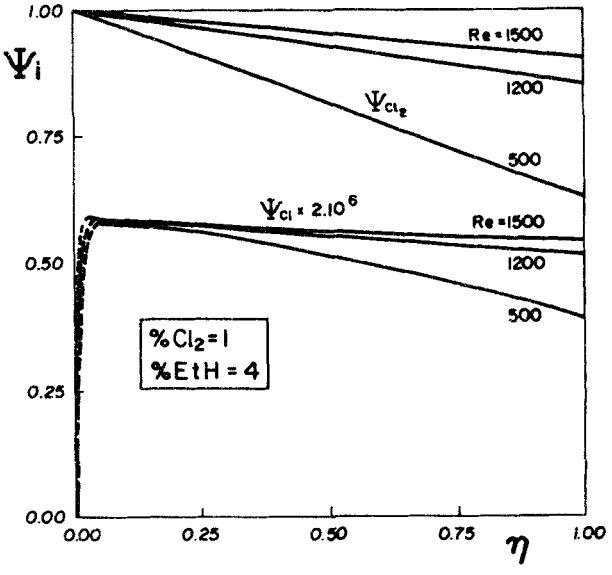

Figure 13. Simulated atomic and molecular chlorine axial concentration profiles.

rine dimensionless concentrations with Re as a parameter. Along the axial coordinate atomic chlorine concentration follows the pattern of the molecular species. Since in the axial direction the irradiation is almost uniform, the influence of the radiation field cannot be observed. The results show why the microsteady-state approximation (MSSA) works well. In spite of an apparently significant change in the axial profile for Ψ_{Cl}, it is clear that more than six orders of magnitude separate the slopes of both curves. The effect of the volumetric flow rate (through changes in Re) is as expected.

It is also clear that the MSSA cannot hold at the entrance of the reactor since the near-constant concentration has not been reached. If the mean residence time of the reactor is too short, the fraction of the reactor volume where the MSSA is not valid will be significant; consequently, predictions of exit conversions could have an important error. This result is directly related to the induction period postulated by Benson (1952) for batch reactor operations.

Figure 14 shows radial profiles at the middle of the reactor ($\eta = 0.5$). The system under analysis may be considered as one with optical thickness ranging from medium to thin. Under these operating conditions some additional information may be drawn about the realtive influence of the radiation field and the fluid velocity field on the reactor performance. For this reactor, the velocity profile influences the shape of the concentration profiles and the conversion of the stable species to a certain extent. Consequently, conversion of Cl_2 is a minimum at the reactor centerline. On the other hand, atomic chlorine very closely follows the pattern of the radiation field, which in optically thin media will concentrate when γ approaches zero. Since concentration of radiation due to the geometry of the system prevails over the attenuation provoked by chlorine absorption, the radiation field is strengthened toward the reactor centerline. At the same time, since the lifetime of atomic chlorine is very short its concentration profile does not follow the shape of that corresponding to molecular chlorine (as in the case of the axial direction) but the variations of the local value of the absorbed energy. Plots of the local volumetric rate of radiant energy

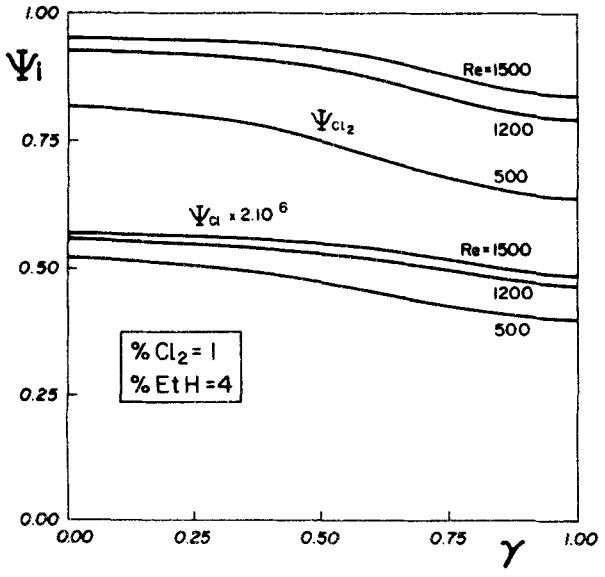

Figure 14. Simulated atomic and molecular chlorine radial concentration profiles.

absorption vs. γ (not shown here) have almost the same shape. Radial concentration profiles for Cl_2 at $\gamma = 1$ do not vary significantly because in our case $r_R = 0.2$ cm and the radiation profile cannot be too steep (Cerdá et al., 1973; Jacob and Dranoff, 1969).

This behavior can be seen in more detail in Figure 15a, which shows the effect of changing the reactor radius. It is seen that when the radius is very small the velocity profile compensates the effect of the radiation distribution and the concentration field is almost flat. Only for intermediate values of r_R does the shape of the velocity field influence the pattern of the chlorine conversion. For larger reactors, the concentration of radiation when γ approaches zero clearly compensates the shorter residence time. In fact, for $r_R = 0.8$ cm the point of maximum conversion has moved toward the wall. Figure 15b shows behavior along the axial coordinate that is consistent with what has been said. It also shows that in a photochemical reactor, even when it is not optically thick, increasing the radius may not be the proper way to increase production. This is a result almost independent of the type of reactor configuration (Romero et al., 1983). It should be remarked that strictly speaking, these conclusions regarding changes in reactor radius are only qualitatively exact because when $r_R/r_L > 0.5$, the assumption of angular symmetry for the mass balance equations is no longer valid (De Bernardez and Cassano, 1982).

Changes in the feed molar ratio and in the volumetric flow rate show an impact similar to that in conventional thermal reactors and they do not need to be discussed here. On the other hand, changes in the chlorine initial concentration produce the expected results in an optically thin photoreactor. Figures 15c

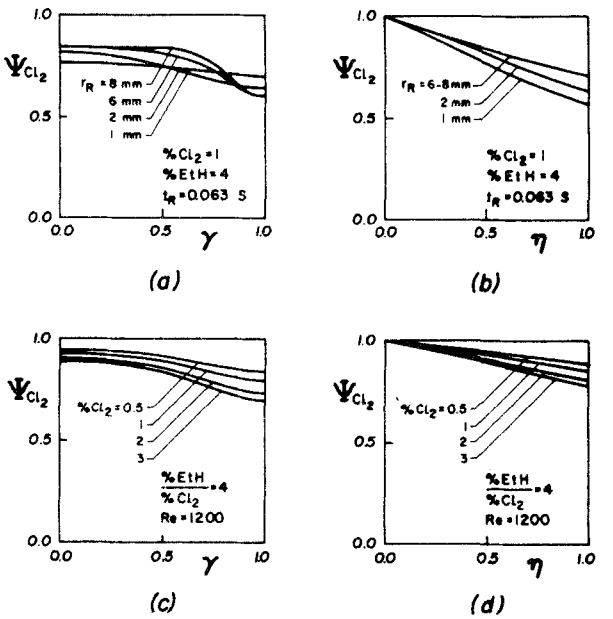

Figure 15. Effects of reactor radius and feed mole fraction.

(a) Effect of reactor radius on chlorine radial concentration profiles; $\eta = 0.5$
(b) Effect of reactor radius on chlorine axial concentration profiles; $\gamma = 0$
(c) Effect of chlorine feed mole fraction on chlorine radial concentration profiles; $\eta = 0.5$
(d) Effect of chlorine feed mole fraction on chlorine axial concentration profiles; $\gamma = 0$

for radial profiles and 15d for axial profiles show that an increase in the chlorine concentration increases conversion; due to the thin optical thickness, radiation penetrates efficiently in the whole reactor volume. It should be noted that this behavior is different from that observed in other systems (mainly liquids), where high values of the optical thickness produce a decrease in the overall exit conversion when the absorbing species concentration is increased. In such systems, radiation penetrates efficiently only to a small fraction of the reactor volume. In fact, under extreme conditions a considerable fraction of the reacting mixture could go through the whole reactor length with no composition changes.

The effect of chlorine concentration can be deduced from Eq. 4. The chlorine concentration enters first as a linear effect and second in a decreasing exponential inside the attenuating integral. For certain values of the optical density number ($\alpha C_{Cl_2} r_R$), the attenuating integral could overcome the effect of the first contribution and the conversion could be decreased.

Note that since the reactor radius also contributes to the value of the optical density number, its effect is felt not only in the Peclet and Reynolds numbers, but in the rate of the initiation step.

Summarizing, the reactor radius and the absorbing reactant concentration are specific photoreactor key parameters in any product yield optimization problem.

Selectivity Studies

In spite of the experimental evidence that in our operating conditions dichlorinated compound concentrations were negligible as compared with the monochloroethane production, some additional computed simulation runs were performed including all possible reaction paths in the reaction mechanism.

With this objective the reaction sequence previously described in Eqs. 8a to 8h was completed with:

$$ClEt + Cl^{\bullet} \underset{k_{-9}}{\overset{k_9}{\rightleftharpoons}} ClEt^{\bullet} + HCl \tag{8i}$$

$$Cl_2 + ClEt^{\bullet} \underset{k_{-10}}{\overset{k_{10}}{\rightleftharpoons}} Cl_2Et + Cl^{\bullet} \tag{8j}$$

$$Cl^{\bullet} + ClEt^{\bullet} \xrightarrow{k_{11}} Cl_2Et \tag{8k}$$

$$ClEt^{\bullet} + ClEt^{\bullet} \xrightarrow{k_{12}} \text{Prod.} \tag{8l}$$

where Cl_2Et is $C_2H_4Cl_2$ and $ClEt^{\bullet}$ stands for $ClC_2H_4^{\bullet}$.

With the same reasoning as before, the reaction on the right-hand side of Eq. 8j will be neglected. Heterogeneous terminations of $ClEt^{\bullet}$ could also have been included. However, their concentration will always be smaller than $Et^{\bullet}$. Consequently, we decided to disregard their participation in the mechanism.

Let us extend our notation and include: $ClEt^{\bullet}(9)$ and $Cl_2Et(10)$.

With the extended mechanism we have added five more reaction steps and two more reacting species. This means one more partial integro-differential equation for $i = 10$ and one more algebraic equation for $i = 9$.

With the exception of the reaction rates for $i = 3$, 5, and 7, all the others described by Eqs. 12 to 18 must be replaced by:

$$\Omega_1 = -J - K_3\Psi_1\Psi_5 - K_{10}\Psi_1\Psi_9 + K_4\Psi_2^2\Psi_8 \tag{47}$$

$$\Omega_2 = 2J - K_2\Psi_2\Psi_3 + K_{-10}\Psi_5\Psi_6 + K_3\Psi_1\Psi_5 - K_9\Psi_2\Psi_4 + K_{-9}\Psi_6\Psi_9 + K_{10}\Psi_1\Psi_9 - K_{11}\Psi_2\Psi_9 - 2K_4\Psi_2^2\Psi_8 - K_5\Psi_2\Psi_5 \tag{48}$$

$$\Omega_4 = K_3\Psi_1\Psi_5 - K_9\Psi_2\Psi_4 + K_{-9}\Psi_6\Psi_9 + K_5\Psi_2\Psi_5 \tag{49}$$

$$\Omega_6 = K_2\Psi_2\Psi_3 - K_{-2}\Psi_5\Psi_6 + K_9\Psi_2\Psi_4 - K_{-9}\Psi_6\Psi_9 \tag{50}$$

and we must add:

$$\Omega_9 = K_9\Psi_2\Psi_4 - K_{-9}\Psi_6\Psi_9 - K_{10}\Psi_1\Psi_9 - K_{11}\Psi_2\Psi_9 - 2K_{12}\Psi_9^2 \tag{51}$$

$$\Omega_{10} = K_{10}\Psi_1\Psi_9 + K_{11}\Psi_2\Psi_9 \tag{52}$$

The MSSA for $i = 2$ and 9 will now be:

$$2K_4\Psi_2^2\Psi_8 + (K_2\Psi_3K_5\Psi_5 + K_9\Psi_4 + K_{11}\Psi_9)\Psi_2 - (2J + K_{-2}\Psi_5\Psi_6 + K_3\Psi_1\Psi_5 + K_{-9}\Psi_6\Psi_9 + K_{10}\Psi_1\Psi_9) = 0 \tag{53}$$

$$2K_{12}\Psi_9^2 + (K_{-9}\Psi_6 + K_{10}\Psi_1 + K_{11}\Psi_2)\Psi_9 - K_9\Psi_2\Psi_4 = 0 \tag{54}$$

while for $i = 5$ Eq. 41 remains unchanged.

Diffusivities were calculated using the same correlations as indicated before. Similarly, we needed additional specific rate constants. They were obtained from reliable data in the literature and are indicated in Table 4.

The performance of the reactor was then again simulated with all these additional reactions incorporated. The following definition will be used:

$$f_2 = \frac{\langle \Psi_{10} \rangle}{\langle \Psi_4 \rangle + \langle \Psi_{10} \rangle} 100 \tag{55}$$

Also, when Eq. 44 is used with the reaction mechanism of Eqs. 8a–8h the exit conversion will be designated as X_m, and when the additional reaction steps, Eqs. 8i–8l, are included, the average exit conversion will be indicated as X_d.

Table 5 shows the results of the manipulation of different operating variables on the formation of dichloroethanes. Although most of these results could have been expected qualitatively, one important fact must be stressed from these results

Table 4. Additional Kinetic Constant Data

Constant	Value $cm^3/mol \cdot s$	Refs.
k_9	$2.62\ 10^{12}$	Chiltz et al. (1963) Cillien et al. (1967)
k_{-9}	$1.97\ 10^{5}$	Chiltz et al. (1963)
k_{10}	$4.61\ 10^{11}$	Kurtz (1972)
k_{-10}	$4.02\ 10^{-2}$	Chiltz et al. (1963)
k_{11}	$2.00\ 10^{14}$	Chiltz et al. (1963)
k_{12}	$1.26\ 10^{13}$	Chiltz et al. (1963)

Table 5. Simulation Results for Selectivity Analysis

(a) % Mole Feed Conc. $Cl_2 = 3$		(b) % Mole Feed Conc. $Cl_2 = 2$; EtH = 4	
% EtH/% Cl_2	f_2	Q, cm^3/s	f_2
0.5	6.73	20.00	1.18
0.75	3.85	26.67	0.97
1.0	2.62	30.00	0.89
2.0	1.12	33.33	0.83
(c) % EtH/% $Cl_2 = 2$		(d) % EtH/% $Cl_2 = 1$	
% Cl_2^0	f_2	% Cl_2^0	f_2
1	0.74	1	1.60
3	1.12	2	2.19
5	1.32	3	2.62
7	1.46	7	3.72

Table 6. Simulation Results: Average Exit Conversions with and without Inclusion of Dichlorinated Compound Formation

	X			
% Cl_2^0	X_m	X_d	$\frac{X_d - X_m}{X_d} \cdot 100$	f_2
1	33.68	34.04	1.06	1.60
2	42.59	43.11	1.21	2.19
3	48.18	48.82	1.31	2.62
7	60.05	60.97	1.51	3.72

$L_R = 30$ cm; $Re = 600$; % EtH/% $Cl_2 = 1$

and from those that were experimentally obtained. All of them indicate that if we do not want to produce secondary products (such as dichlorinated compounds) when the process is carried out photochemically and the appropriate operating conditions are selected, they will not show up. This is not the case for thermal reactions; the main difference is due to the selectivity produced by the low operating temperature permitted by photon-activated reactions.

Table 6 shows the effect of the inclusion of the extended reaction mechanism in the prediction of the average chlorine exit conversions. Clearly, with the definition provided by Eq. 55, the dichloroethane formation is negligible, as shown in the experimental work. Therefore, when monochlorination is the only objective, as long as $C_{C_2H_6}/C_{Cl_2} > 1$, there is no need for the inclusion of steps 8i to 8l in the design of the photoreactor.

All these results strongly suggest that an optimal design of a chlorination photoreactor will surely be able to produce ethyl chloride with a selectivity very close to one.

Conclusions

From our work we can conclude the following.

1. A homogeneous photochemical reactor for chain-type reactions can be rigorously modeled from first principles. All that is needed is:

- Microkinetic information about the reaction
- Physical properties of reactants and products, which should include optical parameters
- Operating characteristics and dimensions of the radiation source, which should include spectral distribution of the lamp output power
- Optical properties of the surface through which radiation enters
- Optical and geometrical properties of reflecting devices, if they are used.

2. There is a strong coupling between the radiation source characteristics and the modeling of the photoreactor, which is translated into the design equations. Thus, to design a photochemical reactor, an iterative procedure will always be required in order to obtain the best combination of reactor parameters and radiation emission system characteristics (with or without reflectors); the main reasons are the unavoidable interactions between the properties of the energy supplier (lamp) and the energy receptor and user (reactor and reacting species).

3. Under all circumstances the radiation balance (which includes an "attenuation integral") is coupled with the mass conservation equations through the reaction rate terms. From the mathematical point of view, this always poses an integro-differential problem. The only exception would be a true photosensitized reaction.

4. Wall (heterogeneous) reactions can safely be neglected in most practical situations. The only possible exception is a reactor operating under a highly turbulent flow with very good radial mixing.

5. Over a critical minimum value of the mean residence time, the local or microsteady-state approximation can safely be used, thus considerably simplifying the design of the photoreactor. This happens when the time needed to reach near-steady concentration of the intermediate species is significantly smaller than the mean residence time of reactants inside the reactor volume.

At the same time, our computer simulation together with our experimental results clearly indicate that:

6. The extense source model produces very accurate predictions of the radiation fields inside photoreactors. This is also true even for complex emission-reflection systems such as the elliptical photoreactor. The significance of this result lies in the fact that this model is derived from the fundamental laws of radiation and requires no experimentally adjustable parameters. Only lamp, reflector, and reactor wall manufacturing specifications and dimensions are needed.

7. A homogeneous continuous photochemical reactor can be satisfactorily designed *a priori*. This is true even for complex chain reactions. The design can be accomplished using the complete reaction mechanism, with reliable microkinetic data obtained from laboratory-scale batch reactors.

8. To obtain good agreement between model predictions and experimental results, a careful purification of reactants and a systematic cleaning of the reactor walls through which the radiation enters are indispensable. This experience singles out some areas of further research work for industrial-scale applications, particularly oriented toward obtaining stable wall conditions.

9. Results indicate that the spectral distribution of the radiation source output power, reactor radius, and radiation-absorbing reactant concentration are specific and unique key parameters for photoreactor optimization. The parametric sensitivity of the last two properties is very different from the one that could be expected for thermal reactions. This is a consequence of the existence of an optimal optical thickness, which is governed by the reactant absorptivity (α), the concentration of the absorbing species (C_{Cl_2}), and the characteristic radiation path length (r_R). They strongly influence the photoreactor performance.

10. A detailed study of the intermediate species concentration profiles shows that they follow the pattern of the stable species from which they are produced in both the axial and radial directions. There is one exception to this: when atomic chlorine is involved, the radial concentration profile is much more closely governed by the profile of the local volumetric rate of energy absorption.

11. Only under certain operating conditions does the fluid velocity field strongly affect the radial concentration profiles. In general its influence is hidden by that of the radiation field.

12. Operating conditions are possible for the selective monochlorination of ethane. A complex optimization procedure will be needed but no additional conceptual difficulties will be involved.

Acknowledgment

The authors are grateful to Omar Brizuela for his participation in the experimental work. They are also grateful to Consejo Nacional de Investigaciones Científicas y Técnicas (CONICET) and Universidad Nacional del Litoral (UNL) for financial aid. Finally, they wish to acknowledge the assistance of Elsa Grimaldi in preparing the English edition of the manuscript.

Notation

a = ellipse semimajor axis, cm
A = area, cm^2
b = ellipse semiminor axis, cm
c = half-distance between focuses, cm
C = concentration, mol/cm^3
d = density, g/cm^3
D = value, Eqs. 4e, 4f, cm
D_{im} = diffusion coefficient for species i, cm^2/s
e = ellipse eccentricity
e^a = local volumetric rate of radiant energy absorption, Einstein/$cm^3 \cdot s$
E = radiant energy flow rate, Einstein/s
f_2 = dichloroethane fraction, Eq. 55
$Ge = r_R/L_R$, geometric number
h = value, Eq. 4c, cm
J = local volumetric rate of radiant energy absorption
k = value, Eq. 4d, cm
k_r = kinetic constant, cm/s (reaction at wall); $cm^3/mol \cdot s$ (second order); $(cm^3)^2/mol^2 \cdot s$ (third order)
K_1 = kinetic initiation number, Eq. 33
K_r = kinetic constants, Eqs. 22–24
L = source, reactor, or reflector length, cm
m = value, Eq. 4h
$Pe_i = \langle v \rangle r_R/D_{im}$, Peclet number for species i
q = radiation flux density, Einstein/$cm^2 \cdot s$
Q = volumetric flow rate, cm^3/s
r = cylindrical radial coordinate, cm
R = reaction rate, $mol/cm^3 \cdot s$
$Re = (d\langle v \rangle 2r_R)/\mu$, Reynolds number
t = residence time, s
$U = v_z/\langle v \rangle$, dimensionless velocity
v = velocity, cm/s
V = source or reactor volume, cm^3
x = Cartesian coordinate, cm
X = chlorine conversion
y = Cartesian coordinate, cm
z = axial coordinate, cm

Greek letters

α = absorption coefficient, cm^2/mol
β = angular cylindrical coordinate, rad
$\gamma = r/r_R$, cylindrical coordinate
Γ = reflection coefficient
$\delta(x - x_i)$ = Dirac delta function
Δ = attenuation distance, Eq. 35
ϵ = variable, Eq. 32
$\eta = z/L_R$, cylindrical coordinate
θ = spherical coordinate, rad
Λ = absorption number
ξ = angle, Eqs. 4e, 4f, rad
ρ = spherical radial coordinate, cm
σ = value, Eq. 4b, cm
Υ = reactor wall transmittance
ϕ = spherical coordinate, rad
Φ = primary quantum yield, mol/Einstein
$\Psi = C/C_i^\circ$, concentration
Ω = reaction rate
μ = viscosity, g/cm · s

Subscripts

d = dichlorination reaction
E = property of a ray emerging from the lamp
exp = experimental value
$exact$ = exact solution
i = species i
I = point of reception or an incident ray property
$init$ = photochemical initiation reaction
j = stable species
L = source
l = unstable species
m = monochlorination reaction
P = point of reflection on elliptical mirror
r = reaction
R = reactor
Rf = reflector
t = theoretical value
SS = MSSA result
w = termination reactions at reactor wall
λ = wavelength of absorption or emission
ν = frequency of absorption or emission
σ = property evaluated at $\lambda = \lambda_\sigma$
o = property evaluated at reactor wall

Superscripts

$'$ = projections on a plane normal to focal axis, also dummy variable
e = outlet section
o = inlet section
$*$ = attenuation path

Special symbols

$\langle\ \rangle$ = average value
$\sim$ = vector
$|\ |$ = absolute value
$\forall$ = "for every value of"

Literature Cited

Alfano, O. M., "Modelado de Foto-reactors Aplicado a Sistemas de más de una Fase y Cinéticas Complejas," Ph.D. Diss., Univ. Nacional del Litoral, Santa Fe, Argentina (1984).

Alfano, O. M., R. L. Romero, and A. E. Cassano, "Radiation Field Inside a Cylindrical Photoreactor Irradiated from the Bottom: Theory and Experiments," *Frontiers in Chemical Reaction Engineering*, Wiley Eastern, New Delhi, v. I, 506 (1984).

Ayscough, P. B., A. J. Cocker, F. S. Dainton, and S. Hirst, "Photochlorination Studies. 6: *cis*-1,2 Dichloroethylene," *Trans. Faraday Soc.*, **58**, 295 (1962).

Baginski, F. C., "Liquid-Phase Photochemical Reactions in a Flow System," D. Eng. Diss., Yale Univ., New Haven, CN (1951).

Benson, S. W., "The Induction in Chain Reactions," *J. Chem. Phys.*, **20**, 1605 (1952).

Bodenstein, M., and W. Unger, "Photochemical Kinetics of Chlorine Detonating Gas. Oxygen-Free Gases," *Z. Physik. Chem.*, **11 B**, 253 (1930).

Boval, B., and J. M. Smith, "Heterogeneous Reactions in the Photochlorination of Propane," *AIChE J.*, **16**, 553 (1970).

Boyd, C. A., N. Stein, V. Steingrimsson, and W. F. Rumpel, "An Interferometric Method of Determining Diffusion Coefficients in Gaseous Systems," *J. Chem. Phys.*, **19**, 548 (1951).
Calvert, J. G., and J. N. Pitts, *Photochemistry*, Wiley, New York (1966).
Cassano, A. E., "Photoreaction Engineering. Chlorination of Propane," Ph.D. Diss., Univ. California, Davis (1968).
Cassano, A. E., and J. M. Smith, "Photochlorination in a Tubular Reactor," *AIChE J.*, **12**, 1124 (1966).
———, "Photochlorination of Propane," *AIChE J.*, **13**, 915 (1967).
Cerdá, J., H. A. Irazoqui, and A. E. Cassano, "Radiation Fields Inside an Elliptical Photoreflector with a Source of Finite Spatial Dimensions," *AIChE J.*, **19**, 963 (1973).
Cerdá, J., J. L. Marchetti, and A. E. Cassano, "Radiation Efficiencies in Elliptical Photoreactors," *Lat. Am. J. Heat Mass Transf.*, **1**, 33 (1977).
Chiltz, G., P. Goldfinger, G. Huybrechts, G. Martens, and G. Verbeke, "Atomic Chlorination of Simple Hydrocarbon Derivatives in the Gas Phase," *Chem. Rev.*, **63**, 355 (1963).
Cillien, C., P. Goldfinger, G. Huybrechts, and G. Martens, "Hydrogen Abstraction from Chlorinate Ethane by Chlorine Atom," *Trans. Faraday Soc.*, **63**, 1631 (1967).
Clariá, M. A., "Metodología para el Diseño *a priori* de Reactores Fotoquímicos en Fase Gas. Monocloración del Etano con Radiación Policromática," Ph.D. Diss., Univ. Nacional del Litoral, Santa Fe, Argentina (1984).
Clark, T. C., and M. A. A. Clyne, "Kinetic Mechanisms in Nitrogen + Chlorine Radical Systems. 2: Kinetics of Elementary Reactions of Nitrogen Trichloride and of the Dichloramino Free Radical," *Trans. Faraday Soc.*, **66**, 372 (1970).
Clyne, M. A. A., and D. H. Stedman, "Recombination of Ground State Halogen Atoms. 2: Kinetics of the Overall Recombination of Chlorine Atoms," *Trans. Faraday Soc.*, **64**, 2698 (1968).
Davis, D. D., W. Braun, and A. M. Bass, "Reactions of Cl $^2P_{3/2}$: Absolute Rate Constants for Reaction with H_2, CH_4, C_2H_6, CH_2Cl_2, C_2Cl_4, and c-C_6H_{12}," *Int. J. Chem. Kinet.*, **2**, 101 (1970).
De Bernardez, E. R., and A. E. Cassano, "Azimuthal Asymmetries in Tubular Photoreactors," *Lat. Am. J. Heat Mass Transf.*, **6**, 333 (1982).
Dickinson, R. G., and J. L. Carrico, "Photochlorination and the Chlorine-Sensitized Photooxidation of Gaseous Tetrachloroethylene," *J. Am. Chem. Soc.*, **56**, 1473 (1934).
Dolan, W. J., C. A. Dimon, and J. S. Dranoff, "Dimensional Analysis in Photochemical Reactor Design," *AIChE J.*, **11**, 1000 (1965).
Fuller, E. N., P. D. Schettler, and J. C. Giddings, "Prediction of Binary Gas-Phase Diffusion Coefficients," *Ind. Eng. Chem.*, **58**, 18 (1966).
Gavalas, G. R., "Long Chain Approximation in Free Radical Reaction Systems," *Chem. Eng. Sci.*, **21**, 133 (1966).
Gebhard, T. J., Ph.D. Diss., Northwestern Univ. Evanston, IL (1978).
Gibson, G. E., and N. S. Bayliss, "Variation with Temperature of the Continuous Absorption Spectrum of Diatomic Molecules. I: Experimental. The Absorption Spectrum of Chlorine," *Phys. Rev.*, **44**, 188 (1933).
Gosselain, P. A., J. Adam, and P. Goldfinger, "La Specificité des Halogenations Atomiques. II: Les Regles Generales qui Determinent le Mecanisme et la Specificité des Halogenations Atomiques," *Bull. Soc. Chim. Belg.*, **65** (1956).
Hanovia Res. Lab. Rept., *Tech. Bull. No. EH-223*, Hanovia Lamp Div., Engelhard Hanovia Inc. (1959).
Harada, J., T. Akehata, and T. Shirai, "Light Intensity Distribution in an Elliptical Photoreactor," *Kagaku Kogaku*, **35**, 233 (1971).
Heraeus Quarzchmelze, *Tech. Bull. No. Q-B1/112 E.*
Herzberg, G., *Molecular Spectra and Molecular Structure. I: Spectra of Diatomic Molecules*, 2nd ed., Van Nostrand Reinhold, New York (1950).
Huff, J. E., and C. A. Walker, "The Photochlorination of Chloroform in Continuous Flow Systems," *AIChE J.*, **8**, 193 (1962).
Hutton, E., and M. Wright, "Photoemissive and Recombination Reactions of Atomic Chlorine," *Trans. Faraday Soc.*, **61**, 78 (1965).
Irazoqui, H. A., J. Cerdá, and A. E. Cassano, "Radiation Profiles in an Empty Annular Photoreactor with a Source of Finite Spatial Dimensions," *AIChE J.*, **19**, 460 (1973).
———, "The Radiation Field for the Point and Line Source Approximations and the Three-Dimensional Source Models: Applications to Photoreactions," *Chem. Eng. J.*, **11**, 27 (1976).
Ivin, K. J., and E. W. R. Steacie, "The Disproportionation and Combination of Ethyl Radicals: The Photolysis of Mercury Diethyl," *Proc. Roy. Soc. London*, **A208**, 25 (1951).
Ivin, K. J., M. H. Wijnen, and E. W. R. Steacie, "Reactions of Ethyl Radicals," *J. Phys. Chem.*, **56**, 967 (1952).
Jacob, S. M., and J. S. Dranoff, "Design and Analysis of Perfectly Mixed Photochemical Reactors," *Chem. Eng. Prog. Symp. Ser.*, **64**, 54 (1968).
———, "Light Intensity Profiles in an Elliptical Photoreactor," *AIChE J.*, **15**, 141 (1969).
Kerr, J. A., and A. F. Trotman-Dickenson, "The Reactions of Alkyl Radicals. III: *n*-Butyl Radicals from the Photolysis of *n*-Valeraldehyde," *J. Chem. Soc.*, **56**, 1602 (1960).
Knox, J. H., and R. L. Nelson, "Competitive Chlorination Reactions in the Gas Phase: Hydrogen and C_1–C_5 Saturated Hydrocarbons," *Trans. Faraday Soc.*, **55**, 937 (1959).
Kramers, W. J., and L. A. Moignard, "The Kinetics of the Photochemical Interaction of Hydrogen with Chlorine," *Trans. Faraday Soc.*, **45**, 903 (1949).
Kurtz, B. E., "Homogeneous Kinetics of Methyl Chloride Chlorination," *Ind. Eng. Chem. Process Des. Dev.*, **11**, 332 (1972).
Matsuura, T., A. E. Cassano, and J. M. Smith, "Acetone Photolysis: Kinetic Studies in a Flow Reactor," *AIChE J.*, **15**, 495 (1969).
Matsuura, T., and J. M. Smith, "Light Distribution in Cylindrical Photoreactors," *AIChE J.*, **16**, 321 (1970).
Noyes, R. M., and L. Fowler, "Mechanisms of Chain Termination in Chlorine Atom Reactions," *J. Am. Chem. Soc.*, **73**, 3043 (1951).
Noyes, W. A., and P. A. Leighton, *The Photochemistry of Gases*, Reinhold, New York (1941).
Pritchard, H. O., J. B. Pyke, and A. F. Trotman-Dickenson, "The Study of Chlorine Atom Reactions in the Gas Phase," *J. Am. Chem. Soc.*, **77**, 2629 (1955).
Reid, R. C., J. M. Prausnitz, and T. K. Sherwood, *The Properties of Gases and Liquids*, 3rd ed., McGraw-Hill, New York (1977).
Rollefson, G. K., *The Photochemistry of Halogens*, Herman, Paris (1938).
Rollefson, G. K., and H. Eyring, "Triatomic Halogen Molecules in Photochemical Reactions," *J. Am. Chem. Soc.*, **54**, 170 (1932).
Romero, R. L., O. M. Alfano, J. L. Marchetti, and A. E. Cassano, "Modeling and Parametric Sensitivity of an Annular Photoreactor with Complex Kinetics," *Chem. Eng. Sci.*, **38**, 1593 (1983).
Schumacher, H. J., "Homogeneous Catalysis by Means of Halogens," *Z. Angew. Chem.*, **50**, 483 (1937).
Spadoni, G., C. Stramigioli, and F. Santarelli, "Rigorous and Simplified Approach to the Modeling of Continuous Photoreactors," *Chem. Eng. Sci.*, **35**, 925 (1980).
Steacie, E. W. R., *Atomic and Free Radical Reactions*, v. I, 2nd ed., Reinhold, New York (1954).
Sylvania Engineering, *Tech. Bull. No. 0-342.*
Tournier, A., X. Deglise, J. C. André, and M. Niclause, "Experimental Determination of the Light Distribution in a Photochemical Reactor," *AIChE J.*, **28**, 156 (1982).
Williams, J. A., "Experimental Observations Concerning the Diffuse, Light Intensity Distribution Model," *AIChE J.*, **22**, 811 (1976).
Williams, J. A., and H. C. Yen, "The Incident Wall Intensity in Elliptical Reflector-Photoreactors," *AIChE J.*, **19**, 862 (1973).
Zolner, W. J., III, and J. A. Williams, "Three-Dimensional Light Intensity Distribution Model for an Elliptical Photoreactor," *AIChE J.*, **17**, 502 (1971).
———, "The Effect of Angular Light Intensity Distribution on the Performance of Tubular Flow Photoreactors," *AIChE J.*, **18**, 1189 (1972).

Manuscript received Mar. 19, 1985, and Aug. 6, 1987.